Journal of Medical and Biological Engineering (2023) 43:258–265
https://doi.org/10.1007/s40846-023-00788-x

ORIGINAL ARTICLE

An Optical Universal Plasmon-Based Biosensor for Virus Detection

Adel Shaaban[1,2] · **Yi-Chun Du**[1,3]

Received: 29 December 2022 / Accepted: 6 April 2023 / Published online: 28 April 2023

Abstract

Purpose Kretschmann-configuration has been used as a subwavelength framework to detect tiny alterations of the refractive index of biomaterials. However, most of the theoretical assessment of such configuration is usually based on the plane wave excitation transfer matrix method (TMM) of prism-coupled to thin metal film supporting plasmonic modes. Accordingly, a better theoretical framework than the plane wave approximation is indispensable for reliable and accurate assessments and simulations. A reformulated form of the traditional FFT-BPM has been adapted to evaluate the performance and characteristics of surface plasmonic waveguide biosensor.

Method Surface plasmon mode is excited by a sub-wavelength narrow light beam. The highly confined optical energy of that plasmonic mode enables an efficient means to detect tiny variations in the composition of the analyte in contact with the metallic layer of the surface plasmon guide. The plasmonic guided power is detected thereafter electronically via an optical MOS capacitor.

Results the guided plasmonic power has been used to assess the fundamental characteristics and performance of the sensor, namely the linearity, sensitivity, and figure of merit as well as the full width at half maximum (FWHM).

Conclusion The proposed sensor could be integrated to a wide class of angular measurement system (for instance goniometer) or via electronic detection of the optical plasmonic guided power. we claim that this work is worthy of being shared with researchers and developers interested in the experimentation and assessment of sensitive biosensors; especially in case when complicated and sophisticated analysis tools represent an unpleasant burden.

Keywords Transfer matrix method (TMM) · Plasmonic waveguide · Biosensor · Waveguides · Full width at half maximum (FWHM)

1 Introduction

Surface plasmon resonance is the collective oscillations of surface electrons at the interface of a dielectric and a metal medium caused by incident electromagnetic radiation. Historically, the first experimental observation of surface plasmon polariton (SPPs) on metals were reported by Wood [1] in early 20th century. He observed the dark and light bands in the reflection spectrum of metallic gratings when transverse magnetic (TM) light beam hit the metallic gratings. This irregular distribution of the dark and light bands was not predicted and explained by theory of diffraction gratings and was known as Wood's anomalies. The presence of viruses (Dengue, Covid-19, etc…) in bio-substances (for instance blood) alter their physical and chemical characteristics [2, 3]. The refractive index is one of the crucial characteristics of the bio-substances [4] which are affected by virus infection. The fast, accurate and reliable detection of the viruses is important for biosensors [5]. Unfortunately, the alteration of the physical characteristics, such as refractive index is usually so minute [6, 7], hence a sensitive and accurate bio-sensor is importance. Optical means of detecting minute changes in the refractive index of fluids is well-known [8–10]. It is well-known for SPP modes, and highly confine the optical energy at the boundary of thin metal film in contact with dielectric materials [11–13].

✉ Yi-Chun Du
terrydu@gs.ncku.edu.tw

[1] Department of Biomedical Engineering, National Cheng Kung University, Tainan 704, Taiwan

[2] Radiation Engineering Department, National Center for Research and Radiation Technology (NCRRT), Egyptian Atomic Energy Authority, Cairo 9621, Egypt

[3] Medial Device Innovation Center, National Cheng Kung University, Tainan 701, Taiwan

This unique peculiarity motivated us to claim that SPP modes excited at the boundary metal/bio-substance could be efficient, accurate and reliable in the detection of minute alterations of refractive index of blood samples due to the infection with viruses (for instance, dengue). Our claim is based on the physical phenomenon of evanescent wave [14], created at boundaries where total reflection occurs. This special type of inhomogeneous waves constitute the core of guided SPP modes at metal/dielectric interface [12]. For instance, Kretschmann-type configuration is one of the most efficient techniques that exploits the evanescent wave resonant excitation of such SPP modes [14]. However, the design and assessment of the bio-sensor performance need an appropriate numerical tool for such evaluations. Unfortunately, the guiding structures of the SPP modes pertain to the sub-wavelength class of optical waveguides [15]. This limits the theoretical frameworks that could be used for such evaluations and assessment [16]. The traditional FFT-BPM [17] is not valid, of course, as the SPP mode is transverse magnetic (TM) in nature. Accordingly, the FFT-BPM has been ignored, in spite of its powerfulness, simplicity and accuracy [18]. Fortunately, [19–21] the traditional FFT-BPM has been revisited and reformulated to handle TM fields recently. Moreover, this renewed version of the FFT-BPM has been applied to some delicate problem, such as butt-coupling between plasmonic and dielectric waveguide [19, 21], and taking into account back-reflected field. This motivated us to tackle the problem under the consideration in this research by the novel framework of FFT-BPM as will be shown.

The integration of plasmon-based device with active and passive plasmonic components has led to fundamental new concepts in the design and implementation of innovative applications in our daily life [19, 22–28]. However, the measurements of guided optical power in plasmonic waveguides were achievable only via optical means [29] until recently Peal et. al. [27] reported an electronic detection method of plasmonic guided power. The concept relies on the optical excitation of free carriers in a semiconductor slab encapsulated between the parallel plates of a MOS capacitor [27, 28]. The evanescent tail of the guided plasmonic mode, (c. f. Figure 1b), penetrates the transparent conductor (TC) (one plate of the parallel plate capacitor) and reaches the semiconductor layer [27]. Consequently, free carriers

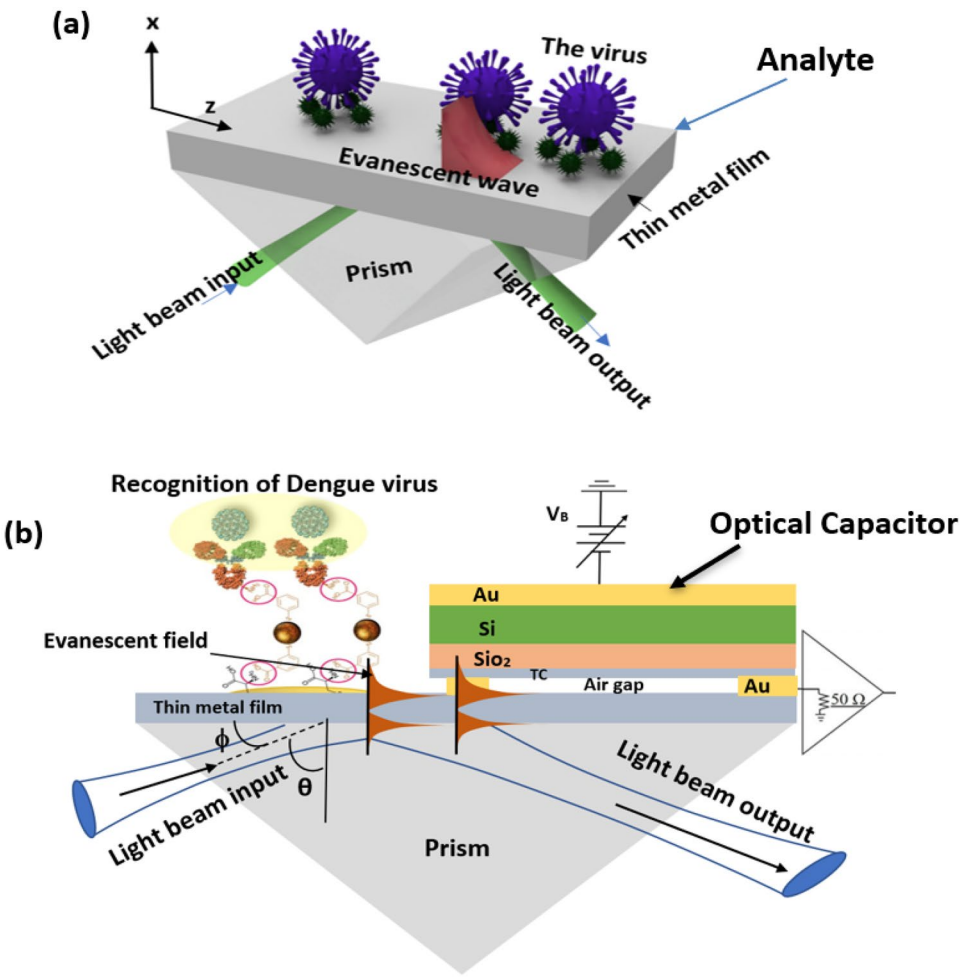

Fig. 1 Schematic of the Kretschmann-configuration plasmon type, **a**) 3D plot, **b**) details of the proposed sensor

are optically excited and subsequently collected through the application of a proper bias voltage V_B as depicted in Fig. 1b. Peal et al. [7], estimated that the best response achieved is 10 mA/W.

Biosensors based on SPP are one of the most promising ones [26]. The surface plasmon resonance (SPR) sensor offers a real time and label free technique for virus detection. It has been used in many virus detection applications, such as: Ebola [28–30], COVID-19 [31–33], Epstein-Barr virus [34, 35], chikungunya virus [36–38], Influenza virus [39–41], and Dengue fever [18, 42, 43]. Here, we present a novel diagnosis scheme based on a hybrid Kretschmann-type configuration integrated as depicted in Fig. 1. In this paper, we consider a detection scheme of dengue virus in human blood samples. Such virus presents a serious risk in more than a hundred of tropical countries [7, 30, 31], which means that almost more than half of earth's population is at direct risk to such disease [30, 32]. Dengue virus infection has many symptoms ranging from acute fever to serious life-threatening effects [13]. Accordingly, fast and accurate diagnosis of dengue virus in its early stages is of prime importance [31, 33]. Unfortunately, traditional diagnosis methods [6] take few days and require expensive equipment [33, 34] which are not appropriate in developing countries suffering from widespread of that disease.

The sensor mechanism is as follows: the power in the metal film is altered because the presence of the dengue antigen in the analyte contiguous to the metal film. Because the specific interaction between the dengue virus and monoclonal antibodies [6, 33, 35], which will effected only by the dengue virus [6, 36], causing a change in the refractive index of the analyte. Higher concentrations of dengue virus results in a corresponding change in the guided power density of the plasmonic mode as depicted in Fig. 2. This indicates that the biorecognition molecules move further apart from the previous binding, and leading to a decrease in the previous binding. The clinical diagnostic of dengue fever virus using SPP has been considered previously [2, 33, 35].

Here, we present a novel diagnosis approach based on a hybrid Kretschmann-type configuration integrated with MOS optical capacitor as depicted in Fig. 1b. The presence of dengue virus in the analyte (blood sample infected by dengue virus). [c.f. Figure 1] alters its refractive index [35, 37, 38] and hence the opto-geometric parameters of the guided mode (for instance: mode profile, propagation constant and optical power density) will be affected subsequently.

The adhesive layer (Ti) has no significant effect on the opto-geometric parameters of the guided plasmonic mode [39]. As the penetration depth of the evanescent tail of the plasmonic mode in the analyte depends strongly on its refractive index [40], such unique property enables a sensitive detection approach for accurate measurement of the concentration of dengue virus in human blood [6, 33].

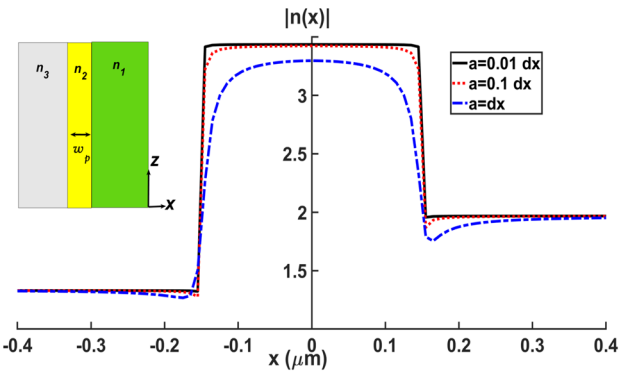

Fig. 2 The refractive index profile using the arctangent smoothing function with different 'a' value

2 Theoretical Considerations

Basically, the biosensor under investigation is a tri-layer (IMI) waveguide as depicted in Fig. 1a. Such waveguide supports a plasmonic mode that is TM in nature [41, 42]. Thus, starting with the TM wave equation for the *y*-component of the magnetic field:

$$\nabla^2 H_y(x,z) + k_0^2 n^2(x) H_y(x,z) - \frac{1}{n^2}\frac{\partial n^2}{\partial x}\frac{\partial H_y}{\partial x} = 0 \tag{1}$$

Obviously the FFT with respect to x of the term $\frac{1}{n^2}\frac{\partial n^2}{\partial x}\frac{\partial H_y}{\partial x}$ represents a major problem when applying the classical FFT-BPM algorithm to TM wave propagation [18].

However, it is possible to transform the TM problem to an equivalent TE one via a transformation of the refractive index profile $n(x)$ of the tri-layer plasmonic waveguide of Fig. 1a to an equivalent one n_{eq} [24]:

$$n_{eq}^2(x) = n^2(x) - \frac{n(x)}{{k_0}^2}\frac{\partial^2}{\partial x^2}\frac{1}{n(x)} \tag{2}$$

This transforms the TM wave equation for the H_y component into the following equivalent TE one [43]:

$$[\nabla^2 + k_0^2 n_{eq}^2] U(x,z) = 0 \tag{3}$$

where $U(x,z) = H_y(x,z)/n(x)$. Obviously, the last term in Eq. (1) involving the product $\frac{\partial n^2}{\partial x}\frac{\partial H}{\partial x}$ is not present in the equivalent TE problem Eq. 3. Hence, the main obstacle preventing the use of FFT-BPM is surmounted via the equivalent refractive index n_{eq} in Eq. 2.

Unfortunately, the second derivative $\frac{\partial^2}{\partial x^2}\frac{1}{n(x)}$ in Eq. 2 represents a major problem especially for a step-like refractive index distribution as in the case of our proposed biosensor (IMI waveguide).

To circumvent the singularity in the second derivative of $\frac{1}{n(x)}$, some smoothing functions are used to approximate the step-like refractive index $n(x)$ [20, 22, 43, 45].

For instance, the arctangent approximation $n_{arc}(x)$ of the original step-index $n(x)$ allows us to write:

$$n_{arc}(x) = n_2 + \left\{ \delta n \left[0.5 + \frac{\tan^{-1}\left(\frac{x}{a}\right)}{\pi} \right] \right\} \tag{4}$$

where n_2 is the ambient (low index) medium, 'a' is the steepness parameter which describes the steepness of the transition of $n(x)$ from n_2 in $x<0$ to $(n_2+\delta n)=n_1$ in $x \geq 0$; it takes on small value compared to the transverse sampling step size Δx, for example $0.1\Delta x$. This is obvious, since as $a \rightarrow 0$, the $n_{\text{arc}}(x)$ tends to an abrupt change from n_1 for $x \geq 0$ to n_2 for $x<0$. Inserting (Eq. 4) in (Eq. 3) we get the equivalent index profile n_{eq}^2 as:

$$n_{eq}^2(x) = n_{arc}^2 - \frac{n_{arc}(x)}{k_0^2}\left[\frac{2(\delta n)^2}{n_{arc}^3(x)\cdot\pi^2 a^2\cdot\left(1+\frac{x^2}{a^2}\right)^2} + \frac{2x\delta n}{n_{arc}^2(x)\cdot\pi a^3\cdot\left(1+\frac{x^2}{a^2}\right)^2}\right] \tag{5}$$

Figure 2 illustrates the effect of the steepness parameter 'a' on the refractive index profile using the arctangent function as an approximation to the step-index waveguide for an IMI waveguide with air core ($n_{\text{co}} = 1$), silver cladding ($n_{\text{cl}} = 0.3970-\text{j}11.4$ at $\lambda = 0.633$ μm) and width $W_p = 50$ nm. Using this approximation some authors [45] studied the surface plasmon modes within the framework of FFT-BPM. Accordingly, surface plasmon modes in a nanostructured Kretschmann arrangement could be assessed easier and simpler than many other methods [14, 47, 48]. In the next section, we compare the results based on FFT-BPM with those based on plane wave resonant reflection coefficient and TMM [6, 7].

3 Numerical Simulation and Assessment of the Performance Parameters

Figure 1b depicts an arrangement of Kretschmann-based biosensor where a thin gold (Au) film is deposited on the base of a glass prism with high refractive index $n_p = 1.969$. The complex refractive index of gold at $\lambda = 633$ nm is $n_m = 0.18344+\text{j}3.4332$ [48]. The thickness of the gold film $d = 50$ nm. The *virus-free* analyte normal blood sample has a refractive index $n_a = 1.33$. Based on minimum reflectance [7], a *plane wave* at $\lambda = 633$ nm will excite the plasmonic mode (cf. Figure 1b) when it is incident on the prism base at the resonance angle $\theta_{i1} = 47.1272°$ [angle of minimum reflectance]. The superiority of the FFT-BPM stems from the fact that, by a simple adjustment of the width W of the "narrow" incident light *beam*, for instance near-wavelength or sub-wavelength rectangular pulse, the excitation of the plasmonic mode becomes quite easy [49, 51], and does not need a sharp adjustment of the incidence angle θ_i as it should be in the traditional plane wave excitation [51, 53]. Such spatially limited light beam having sufficient spectral extent of plane waves is capable to fulfil the resonance condition, without the need to readjust the angle of incidence for each value of the analyte refractive index n_{a}.

An example of the capability of the FFT-BPM is shown in Fig. 3a, it illustrates the evolution of the magnitude of the total propagated magnetic field $\text{H}_\text{y}(\text{x})$ of a unity amplitude rectangular pulse as it propagates in the z-direction. The pulse width $W = 0.5\lambda$ is incident from the prism on the metal film with the analyte overlay such that total reflection on the prism-metal interface is satisfied [29]. The pulse is centered at $x_c = W$ from the prism-metal interface. The pulse is launched at the plane $z = 0$ with a tilt angle $\phi = 42.377°$ with respect to the z-axis. The inset shows a close-up of the modal plasmonic field as it evolves inside the metal film. Figure 3b shows the profile of the plasmonic mode in the $\text{z} = 0.35$ μm, half-way the total propagation distance $Z_{\text{t}} = 0.7$ μm. The parameters of the FFT-BPM take on the following values: transverse sampling interval $\Delta x = 0.1$ nm, free space wavelength $\lambda = 633$ nm, total number of sampling points $N_x = 2^{16}$, and propagation step size $\Delta z = 0.5$ nm.

We considered three practical values for the analyte [6, 7, 33]: a lower positive blood sample (dengue-sero2) corresponding to $n_{\text{a2}} = 1.33691$ [7, 33], where the plasmonic mode occurs at an excitation angle $\theta_{i2} = 47.5066°$. A mid-positive sample (dengue-sero3) has a refractive index $n_{a3} = 1.33909$ with an excitation angle $\theta_{i3} = 47.627°$, and a high-positive sample (dengue-sero4) corresponding to $n_{a4} = 1.3405$ will be excited at an angle $\theta_{i4} = 47.7051°$. Obviously, the plane wave excitation of the plasmonic mode over the whole range of the analyte index n_a, requires an accurate readjustment (fraction of a degree) of θ_i for each value of n_a. This is impractical, as the dip in the reflectance curve (resonance of the plasmonic mode) is quite sharp [4, 42, 54]; consequently, this requires a highly skilled person or a sophisticated automatic opto-mechanical control system to search accurately for the angle of minimum reflectance [9].

$$k_{xi} = k_o n_p \sin\phi_i = k_o n_p \cos\theta_i \tag{6}$$

$$\therefore k_{zi} = \sqrt{k_o^2 n_p^2 - k_{xi}^2} = k_o n_{eff} = k_o n_p \cos\phi_i = k_o n_p \sin\theta_i \tag{7}$$

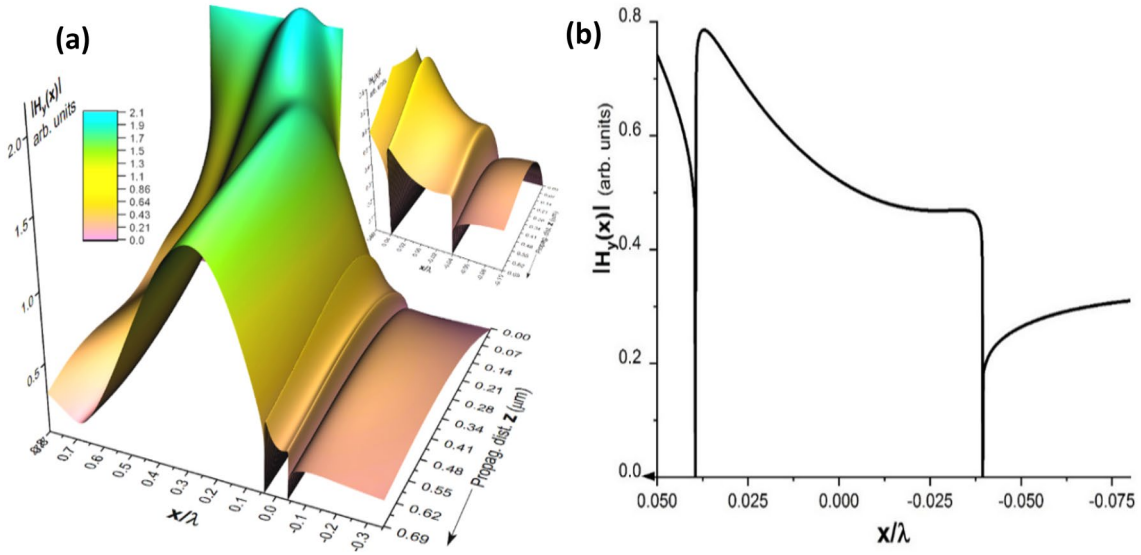

Fig. 3 **a** 3D plot for the propagated field and the inset shows the modal field in the metal film. **b** The magnitude of the magnetic field inside and around the metal film at the plane $z=0.35$ micron, where the magnitude of the plasmonic mode reaches its maximum value

$$\therefore \sin\theta_i = \frac{n_{eff}}{n_p} \approx \frac{1}{n_p}\mathrm{Re}\left\{\sqrt{\frac{\varepsilon_a\varepsilon_m}{\varepsilon_a+\varepsilon_m}}\right\} \tag{8}$$

Hence, it is of prime importance to avoid such critical readjustment of the angle of incidence. Fortunately, this is possible within the framework of the FFT-BPM, since by properly choosing the width W of the "spatially limited" incident light *beam* (cf. Figure 1b), the excitation of the plasmonic mode becomes quite easy, over the whole range of n_a. This is easily satisfied when the spatial spectrum $w(k_x)$ (plane wave expansion) of that narrow beam has a spectral component k_{xi} that satisfies the resonance condition of the plasmonic mode [8, 54]:

Where n_{eff} is the effective index of the guided plasmonic mode in the tri-layer (IMI) waveguide [41, 42, 54]. ε_m and ε_a being the relative dielectric constant of the analyte and metal film, respectively. For instance, a rectangular pulse with unity amplitude and width W, has a spatial spectrum $w(k_x)$ (plane wave expansion) given by the spatial Fourier transform [55]:

$$w(k_x) = W\frac{\sin(k_xW/2)}{k_xW/2} \tag{9}$$

where the variable of the Fourier transform k_x, is the transverse component of the wave vector of a representative plane wave in the spatial spectrum of the incident beam. With such narrow light beam, the fundamental parameters of the proposed detection scheme could be investigated and assessed accurately and easily such as the linearity, sensitivity (Si) and figure of merit (FOM).

A criterion for the linearity of the suggested sensor is the variation of the guided plasmonic modal power density P_g as function of the analyte refractive index n_a [56]. Such power is measurable directly via the optical MOS capacitor described in [27].

Figure 4 illustrates the spatial spectrum of the magnetic field of the exciting narrow beam $H_y(k_x)$ (proportional to a Sinc function (Eq. 9) that is incident on the prism base at an angle $\theta=47.622°$ corresponding to $k_x/k_o = 1.327$ where the normalized spectrum attains its peak value (cf. the excitation line in the inset in Fig. 4). This value does *not* correspond to any resonant angle θ_i of the plasmonic modes for the three dengue-sero samples. The idea is to check that the

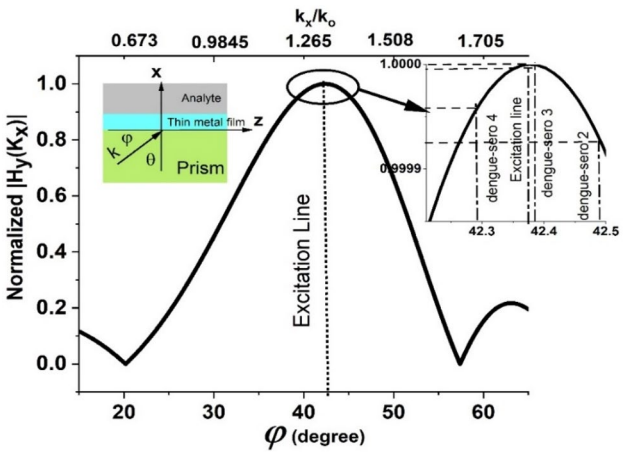

Fig. 4 Spectrum of the narrow incident beam on the base of the prism at $\theta=\pi/2-\varphi=47.6^{o}$

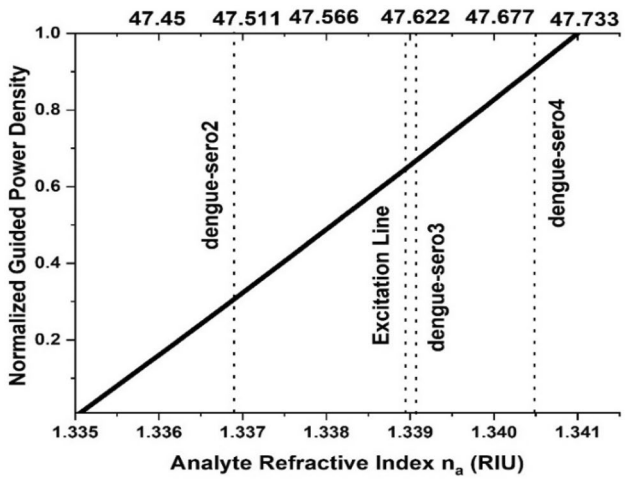

Fig. 5 Sensor linearity over the entire range of n_a

excitation efficiency of the plasmonic modes corresponding to the whole range of n_a is *independent* of the incidence angle θ_i of the narrow light beam, thus all the modes are excited almost equally likely as seen in the inset of Fig. 4; which reveals the magnitude of the Fourier transform $|H_y(k_x)|$ (spatial spectrum) of the rectangular pulse. Evidently, the values of $|H_y(k_x)|$ corresponding to dengue-sero 2, 3 and 4 are almost equal as the vary negligibly around 1 (the peak of the Sinc-function). The spectrum $H_y(k_x)$ is quite wide such that the variation of $|H_y(k_x)|$ around the spectral component $k_x/k_o = 1.327$ (corresponding to $\theta = 42.38°$) is so tiny (over the whole range of n_a corresponding to a variation in the resonance angle from 42.2° to 42.5°) as revealed in the inset. This confirms that it is unnecessary to readjust θ_i for each value of the analyte n_a. This is one of the fundamental advantages of the FFT-BPM from the practical point of view, especially during the design and assessment phases of the proposed sensor and many other types of biosensors as well [57, 59].

The main performance characteristics of an SPR-based sensor is the linearity, sensitivity, and figure of merit. The linearity of the proposed sensor could be defined as the change of the guided power inside the metal film as function of the analyte refractive index. Figure 5 shows the change of the normalized guided power density (P_g) with the analyte refractive index. The figure reveals a fair linearity of P_g with the analyte refractive index n_a. The upper axis depicts the resonance angle θ_i corresponding to n_a. The dashed lines depicts the resonance angles corresponding to the practical values of n_a for each value of the dengue-sero samples.

The sensitivity S_i, defined as the change in the modal plasmonic guided power density ΔP_g per unit change in the analyte refractive index unit (RIU) [8] $S_i = \Delta P_g/\Delta n_a$ is almost 167 per RIU. On the other hand, the angular sensitivity $S_\theta = \Delta P_g/\Delta\theta_i \approx$ 3.5 per degree, which is comparable to the value 3.427 of an enhanced measurement scheme [59]. An appropriate Figure of merit FOM of the proposed sensor can be defined as the ratio between the sensitivity and the width W of the exciting incident pulse ($W = 0.5\lambda$) that is: $FOM_i = S_i/W \approx 528$ per RIU/μm [8].

4 Conclusion

The modified FFT-BPM has been applied successfully to investigate and assess the performance of a plasmonic-based biosensor as a diagnosis tool for blood infected by dengue virus. The proposed sensor could be integrated with an optical MOS capacitor to enable fast and direct electronic detection of dengue fever virus. The measurable parameter is taken to be the plasmonic guided power to get benefit from the optical MOS capacitor which enables direct conversion of guided optical power to electrical current. The integration of the Kretschmann-based configuration with the optical MOS capacitor allows the realization of a feasible device. Compared with other measurement schemes, the proposed sensing method reveals fair linearity, as well as a competitive sensitivity and figure of merit.

Acknowledgements The authors thanks Prof. Lotfy Rabeh Gomaa for his suport and guidance throughout this research. During the research Prof. Lotfy provided valuable insights and recommendations that greatly enhanced the quality of this work.

Author Contributions AS conceptualization, formal analysis, investigation, writing–original draft, YCD Conceptualization, formal analysis, investigation, review, and editing.

Funding This work was supported in part by the National Science and Technology Council, Taiwan, under Grant 111-2622-E-006-007 and 110-2221-E-006-087-MY3.

Data Availability All data generated or analyzed during this study are included in this manuscript.

Declarations

Competing Interests The authors declare no competing interests regarding this manuscript.

Ethical Approval The study was performed following the principles outlined in the Helsinki Declaration (IRB Number: KSVGH21-CT11-11(210629-1)).

Consent to Participate No requirement for informed consent for this study.

Consent to Publish Not applicable.

References

1. Wood, R. W. (1901). On a remarkable case of uneven distribution of light in a diffraction grating spectrum. *Proceedings of the Royal*

Society of London, 18(1), 269–275. https://doi.org/10.1088/1478-7814/18/1/325
2. Mariani, S., & Minunni, M. (2014). Surface plasmon resonance applications in clinical analysis. *Analytical And Bioanalytical Chemistry*, *406*, 2303–2323.
3. Park, J. H., Cho, Y. W., & Kim, T. H. (2022). Recent advances in surface plasmon resonance sensors for sensitive optical detection of pathogens. *Biosensors*, *12*(3), 180.
4. Homola, J. (2006). *Surface plasmon resonance based sensors*. Springer Science & Business Media.
5. Martina, B. E. E., Koraka, P., & Osterhaus, A. D. M. E. (2009). Dengue virus pathogenesis: An integrated view. *Clinical Microbiology Reviews, 22*(4), 564–581. https://doi.org/10.1128/CMR.00035-09
6. Jahanshahi, P., Zalnezhad, E., Sekaran, S. D., & Adikan, F. R. M. (2014). Rapid immunoglobulin M-based dengue diagnostic test using surface plasmon resonance biosensor. *Scientific Reports*, *4*, 3851.
7. Jahanshahi, P., Sekaran, S. D., & Adikan, F. R. M. (2015). Optical and analytical investigations on dengue virus rapid diagnostic test for IgM antibody detection. *Medical & Biological Engineering & Computing*, *53*(8), 679–687.
8. Gupta, B. D., Srivastava, S. K., & Verma, R. (2015). *Fiber optic sensors based on plasmonics*. World Scientific.
9. Homola, J., Yee, S. S., & Gauglitz, G. (1999). Surface plasmon resonance sensors: Review. *Sensors Actuators B Chemistry, 54*(1), 3–15. https://doi.org/10.1016/S0925-4005(98)00321-9
10. Čtyroký, J., Homola, J., & Skalský, M. (1997). Tuning of spectral operation range of a waveguide surface plasmon resonance sensor. *Electronics Letters*, *33*, 1246–1248. https://doi.org/10.1049/el:19970814.
11. Enoch, S., & Bonod, N. (2012). *Plasmonics: From basics to advanced topics*. Springer.
12. Kik, P. G., & Brongersma, M. L. (2007). *Surface plasmon nanophotonics*. Springer.
13. Maier, S. A. (2007). *Plasmonics: Fundamentals and applications*. Springer.
14. Raether, H. (1988). Surface plasmons on smooth surfaces. *Surface plasmons on smooth and rough surfaces and on gratings* (pp. 4–39). Springer.
15. Berini, P. (2000). Plasmon-polariton modes guided by a metal film of finite width bounded by different dielectrics. *Optics Express*, *7*(10), 329. https://doi.org/10.1364/oe.7.000329.
16. Veronis, G., & Fan, S. (2007). Theoretical investigation of compact couplers between dielectric slab waveguides and two-dimensional metal-dielectric-metal plasmonic waveguides. *Optics Express*, *15*(3), 1211. https://doi.org/10.1364/oe.15.001211.
17. Feit, M. D., & Fleck, J. A. (1978). Light propagation in graded-index optical fibers. *Applied Optics*, *17*(24), 3990–3998.
18. Vassallo, C. (1997). Difficulty with vectorial BPM. *Electronics Letters*, *33*(1), 61–62. https://doi.org/10.1049/el:19970014.
19. Shaaban, A., Du, Y. C., & Gomaa, L. R. (2019). Transmissivity assessment of plasmonic-dielectric waveguide interconnects via modified FFT-BPM. *Optik (Stuttg), 208*, 164143
20. Shaaban, A., Du, Y. C., & Gomaa, L. R. (2021). Effects of smoothing functions on the transformation of TM to TE propagation problems in the framework of FFT-BPM: A comparative study. *Optics Communication*, *478*, 126374.
21. Shaaban, A., Du, Y. C., & Gomaa, L. R. (2019). Extension of an FFT-based beam propagation method to plasmonic and dielectric waveguide discontinuities and junctions. *Applied Sciences, 9*(20), 4362.
22. Gomaa, L. R., Shaaban, A., Hameed, M. F. O., & Obayya, S. S. A. (2017). Competitiveness of the BPM in studying the optical beams at critical incidence on dielectric interfaces. *Optical and Quantum Electronics*. https://doi.org/10.1007/s11082-016-0886-2
23. Shaaban, A., Du, Y. C., & Gomaa, L. R. (2019). Extension of an FFT-based beam propagation method to plasmonic and dielectric waveguide discontinuities and junctions. *Applied Sciences*. https://doi.org/10.3390/app9204362
24. Shaaban, A., et al. (2019). Fast parallel beam propagation method based on multi-core and many-core architectures. *Optik (Stuttg)*. https://doi.org/10.1016/j.ijleo.2018.11.111
25. Shaaban, A., Hameed, M. F. O., Gomaa, L. R., & Obayya, S. S. A. (2018). Accurate calculation of Goos-Hänchen shift at critical angle for complex laser beam profiles using beam propagation method. *Optik (Stuttg)*. https://doi.org/10.1016/j.ijleo.2017.11.184
26. Zakharian, A. R., Moloney, J. V., & Mansuripur, M. (2007). Surface plasmon polaritons on metallic surfaces. *Optics Express*, *15*(1), 183–197.
27. Peale, R. E., et al. (2016). Electronic detection of surface plasmon polaritons by metal-oxide-silicon capacitor. *APL Photonics*, *1*(6), 66103.
28. Bora, M., Çelebi, K., Zuniga, J., Watson, C., Milaninia, K. M., & Baldo, M. A. (2009). Near field detector for integrated surface plasmon resonance biosensor applications. *Optics Express*, *17*(1), 329–336.
29. Homola, J. (2006). *Surface plasmon resonance based sensors*. Springer.
30. S. European Centre for Disease Prevention and Control. (2022). *Dengue worldwide overview*. ECDC). https://www.ecdc.europa.eu/en/dengue-monthly.
31. Anusha, J. R., Kim, B. C., Yu, K. H., & Raj, C. J. (2019). Electrochemical biosensing of mosquito-borne viral disease, dengue: A review. *Biosensors & Bioelectronics*, *142*, 111511. https://doi.org/10.1016/j.bios.2019.111511.
32. Shaaban, A., Du, Y. C., & Gomaa, L. R. (2020). Integrated sensitive surface plasmon biosensor for dengue-fever detection. doi: https://doi.org/10.1109/ICP46580.2020.9206504.
33. Wong, W. R., Krupin, O., Sekaran, S. D., Mahamd Adikan, F. R., & Berini, P. (2014). Serological diagnosis of dengue infection in blood plasma using long-range surface plasmon waveguides. *Analytical Chemistry*, *86*(3), 1735–1743.
34. Shaaban, A., Du, Y. C., & Gomaa, L. (2020). Integrated sensitive biosensor with surface plasmon for dengue fever detection. Mar.
35. Eivazzadeh-Keihan, R., et al. (2019). Dengue virus: A review on advances in detection and trends–from conventional methods to novel biosensors. *Microchimica Acta*, *186*(6), 329.
36. Omar, N. A. S., Fen, Y. W., Abdullah, J., Chik, C. E. N. C. E., & Mahdi, M. A. (2018). Development of an optical sensor based on surface plasmon resonance phenomenon for diagnosis of dengue virus E-protein. *Sensing and Bio-Sensing Research, 20*, 16–21.
37. Kuhn, R. J., et al. (2002). Structure of dengue virus: implications for flavivirus organization, maturation, and fusion. *Cell, 108*(5), 717–725. https://doi.org/10.1016/S0092-8674(02)00660-8
38. Roy, S. K., & Bhattacharjee, S. (2021). Dengue virus: Epidemiology, biology, and disease aetiology. *Canadian Journal Of Microbiology*, *67*(10), 687–702. https://doi.org/10.1139/cjm-2020-0572.
39. Jahanshahi, P., Ghomeishi, M., & Adikan, F. R. M. (2012). "Adhesive layer effect on gold-silica thin film interfaces for surface plasmon resonance modeling," In *IEEE 3rd International conference on photonics*, 2012, pp. 89–92. doi: https://doi.org/10.1109/ICP.2012.6379841.
40. Bhatia, P., & Gupta, B. D. (2013). Surface plasmon resonance based fiber optic refractive index sensor utilizing silicon layer: Effect of doping. *Optics Communication*, *286*, 171–175. https://doi.org/10.1016/j.optcom.2012.08.097.
41. Berini, P. (2009). Long-range surface plasmon polaritons. *Advances in Optics and Photonics*. https://doi.org/10.1364/AOP.1.000484

42. Sophocles, J. O. (2003). *Electromagnetic waves and antennas*. Rutgers Press.
43. Poladian, L., & Ladouceur, F. (1998). Unification of TE and TM beam propagation algorithms. *Ieee Photonics Technology Letters*, *10*(1), 105–107.
44. Shaaban, A., Hameed, M. F. O., Obayya, S. S. A., Gomaa, L. R., & Swillam, M. A. (2017). Modified BPM for plasmonic modeling. doi: https://doi.org/10.23919/ROPACES.2017.7916399.
45. Čtyroký, J., et al. (1999). Theory and modelling of optical waveguide sensors utilising surface plasmon resonance. *Sensors Actuators B Chem*, *54*(1), 66–73. https://doi.org/10.1016/S0925-4005(98)00328-1.
46. Gupta, B. D., & Verma, R. K. (2009). Surface plasmon resonance-based fiber optic sensors: Principle, probe designs, and some applications. *Journal of Sensors*. https://doi.org/10.1155/2009/979761
47. Phillips, K. S., & Cheng, Q. J. (2008). Surface plasmon resonance. Molecular Biomethods Handbook. doi:https://doi.org/10.1007/978-1-60327-375-6_46.
48. Johnson, P. B., & Christy, R. W. (1972). Optical constants of the noble metals. *Physical Review. B, Condensed Matter*, *6*(12), 4370.
49. Oulton, R. F., Bartal, G., Pile, D. F. P., & Zhang, X. (2008). Confinement and propagation characteristics of subwavelength plasmonic modes. *New Journal Of Physics*, *10*(10), 105018.
50. Veronis, G., & Fan, S. (2007). Modes of subwavelength plasmonic slot waveguides. *J Light Technol*, *25*(9), 2511–2521.
51. Diouf, M., Burrow, J. A., Krishna, K., Odessey, R., Abouraddy, A. F., & Toussaint, K. C. (2022). Excitation of surface plasmon polaritons by diffraction-free and vector beams. *Applied Optics*, *61*(25), 7469–7473.
52. Popov, E., Bonod, N., Nevière, M., Rigneault, H., Lenne, P. F., & Chaumet, P. (2005). Surface plasmon excitation on a single subwavelength hole in a metallic sheet. *Applied Optics*, *44*(12), 2332–2337. https://doi.org/10.1364/AO.44.002332.
53. Homola, J., Koudela, I., & Yee, S. S. (1999). Surface plasmon resonance sensors based on diffraction gratings and prism couplers: Sensitivity comparison. *Sensors Actuators B Chemistry, 54*(1), 16–24. https://doi.org/10.1016/S0925-4005(98)00322-0
54. Liu, C., et al. (2020). Fiber SPR refractive index sensor with the variable core refractive index. *Applied Optics*, *59*(5), 1323–1328.
55. Ersoy, O. K. (2006). *Diffraction, fourier optics and imaging*. John Wiley & Sons.
56. Vinogradov, A. P., Dorofeenko, A. V., Pukhov, A. A., & Lisyansky, A. A. (2018). Exciting surface plasmon polaritons in the Kretschmann configuration by light beam. *Physical Review B, 97*(23), 235407
57. Shibayama, J., Takeuchi, T., Goto, N., Yamauchi, J., & Nakano, H. (2007). Numerical investigation of a Kretschmann-type surface plasmon resonance waveguide sensor. *Journal of Lightwave Technology, 25*(9), 2605–2611. https://doi.org/10.1109/JLT.2007.903823
58. Shaaban, A., Du, Y. C., & Gomaa, L. R. (2020). Integrated Sensitive Surface Plasmon Biosensor for Dengue-fever Detection. *2020 IEEE 8th Int. Conf. Photonics, ICP 2020*, doi:https://doi.org/10.1109/ICP46580.2020.9206504.
59. Lee, K. S., Son, J. M., Jeong, D. Y., Lee, T. S., & Kim, W. M. (2010). Resolution enhancement in surface plasmon resonance sensor based on waveguide coupled mode by combining a bimetallic approach. *Sensors (Basel, Switzerland)*, *10*(12), 11390–11399.